J Comput Electron (2014) 13:496–502
DOI 10.1007/s10825-014-0560-5

Effect of unit-cells of the frequency selective surface as superstrate on the directivity of rectangular microstrip antenna

Kumud Ranjan Jha · G Singh

Published online: 20 February 2014

Abstract In this paper, the relationship between the number of unit-cells used in the design of a frequency selective surface (FSS) and its expected directivity is established. The relationship between the number of FSS unit-cells and the directivity is based on the planer microstrip patch array antenna design concept where the unit-cell is treated as the superstrate illuminated by the source. To validate the proposed technique, the analytical value of the directivity has been compared with that of ray-tracing method. The directivity of antenna is calculated for two different planar array configurations at 600 GHz. The results of numerical analysis are compared to that of the full-wave electromagnetic simulator CST Microwave Studio and results are comparable. Further, the directivity computed by this proposed technique has also been compared with that of the reported in literatures.

Keywords Microstrip antenna · Directivity · Uniform planar array · Frequency selective surface

1 Introduction

Simple probe-fed microstrip patch antenna suffers from the poor directivity [1] which can be enhanced by using a highly reflective surface as the superstrate [2]. In general, the directivity of the antenna increases due to the collimation of the electromagnetic field in the intended direction. The radiation of electromagnetic field is due to the leakage of the energy from inter-frequency- selective- surface gaps and this kind of the antenna can be modeled as the leaky wave antenna [3]. However, a list of the computation methods of this kind of the antenna is documented in [4].

Recently, on the basis of the various modeling techniques, the cavity resonator antennas (CRA) have extensively been studied at the microwave and millimeter wave frequencies [5–14] to enhance the gain and directivity of the antenna. However, there is the similarity among all these studies that the size of the superstrate is comparatively large and semi-infinite superstrate has been used in analysis. Apart from the microwave and millimeter-wave, there is also the demand of highly directive antennas at terahertz frequency for various applications like imaging and sensing [15]. Further, to meet the future demand of the wide bandwidth, there is the need to enhance the operating frequency of the antenna to terahertz regime of the electromagnetic spectrum [16] and at this frequency, due to the heavy path-loss [17], significantly high directivity antennas are required [18]. At the high frequency (millimeter and terahertz), number of antennas have been reported in literature [19–26] but they all cannot be used in the system-on-chip design. Due to the on-planar configuration capability, the microstrip antennas find potential applications at the terahertz frequencies [27].

However, either at the microwave/millimeter wave or terahertz frequency, the directivity of the CRA antenna is influenced by the number of unit-cells used in the array, its geometry and the periodicity of the unit-cell. In general, the size of the superstrate is considered to be large but the exact relationship between the number of unit-cells and the achieved directivity at the chosen resonance frequency has not been investigated.

K. R. Jha
School of Electronics and Communication Engineering, Shri Mata Vaishno Devi University, Katra, Jammu and Kashmir, India
e-mail: jhakr@rediffmail.com

G. Singh (✉)
Department of Electronics and Communication Engineering, Jaypee University of Information Technology, Solan, Himachal Pradesh, India
e-mail: drghanshyam.singh@yahoo.com

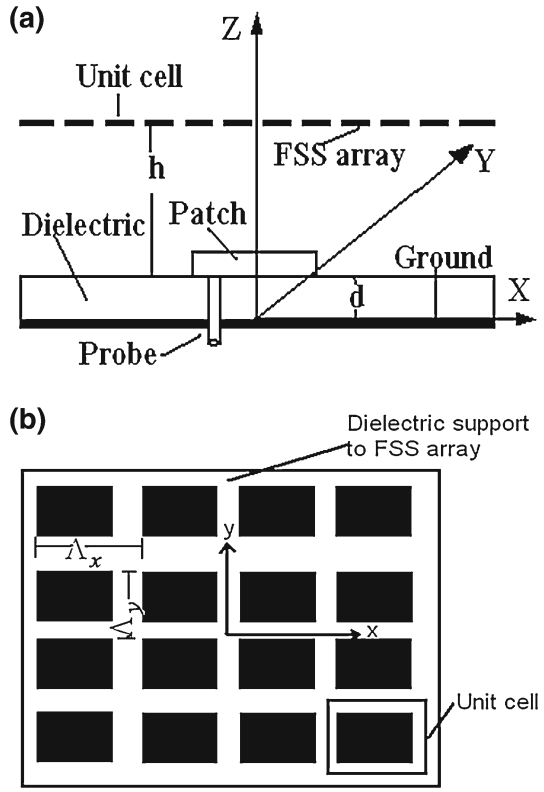

Fig. 1 Schematic of the **a** *side-view* of a probe-fed microstrip antenna with superstrate and **b** *top-view* of the FSS superstrate

In this paper, we have established a relationship between numbers of unit-cells used in CRA to the directivity of the antenna using the two-dimensional planar array technique. The manuscript is organized in the following manner. The Sect. 2 deals with the theory of operation of the proposed antenna. Section 3 predicts the directivity of the proposed antenna at terahertz frequency. The Sect. 4 deals with the comparison of the directivity of antenna with recently reported literature at microwave frequency. Finally, the Sect. 4 concludes the work.

2 Theory of operation

The schematic diagram of a microstrip patch antenna with FSS as superstrate is shown in Fig. 1.

In Fig. 1a, the side-view of a rectangular microstrip patch antenna with FSS as superstrate is shown. In this figure, a simple patch of physical length (L) and width (W) is placed on a dielectric substrate of thickness 'd'. The patch is exited by a cylindrical probe of radius r. A metallic FSS array working as superstrate as shown in Fig. 1b is placed at height 'h' above the substrate and supported by dielectric material. The thickness and dielectric permittivity of the substrate and that support to the FSS are same. The thickness of the ground plane, radiating patch and FSS array is same and it is equal to 't' and the periodicity of the FSS unit-cell along x- and y-axis is Λ_x and Λ_y, respectively. The analysis of this kind of the antenna involves the prediction of the resonant height of the cavity and the peak directivity of the antenna using the unit-cell model of the FSS at the resonant height [28]. However, for other than peak directivity, the analysis is divided into two parts as: (a) calculation of the resonant height of the cavity and (b) establishing the relationship between the number of unit-cells to the beam-width and directivity of the FSS array superstrate antenna.

2.1 Resonant height

The resonant height of the FSS superstrate antenna is predicted with the help of resonance estimation using the ray-tracing technique which has been frequently used in the past. The resonance condition for the antenna structure at bore-sight angle and the operating frequency at height of the superstrate above the substrate is obtained as [28]:

$$h = \frac{N\lambda}{2} + \left(\frac{\phi_g + \phi_{FSS}}{\pi}\right)\frac{\lambda}{4} \qquad N = 1, 2, 3\ldots\ldots \tag{1}$$

In Eq. (1), N, λ, ϕ_g and ϕ_{FSS} are the integer numbers, free-space wavelength, reflection phase angle of the ground plane and reflection phase angle of the superstrate unit-cell, respectively. The value of ϕ_g is obtained by using the following formula.

$$\phi_g = \pi - 2\tan^{-1}\left(\frac{Z_d \tan(\beta d)}{Z_0}\right) \tag{2}$$

In the Eq. (2), Z_d, Z_0 and β are the characteristics impedance of the wave in dielectric substrate, characteristic impedance of the wave in free-space and the phase constant of the wave in the substrate, respectively.

2.2 Directivity

In general, the directivity of FSS array is described by evaluating the phase angle and the magnitude of the reflection coefficient (Γ) of the unit-cell of array [29] which considers the array of semi-infinite length. However, for the finite number of unit-cells, with the small discrepancies, the planar array concept [30] may be used to calculate the directivity. In this way, by knowing the value of directivity, the number of unit-cells can be decided or from the knowledge of unit-cells, the directivity may be calculated. In the planar antenna array, the illumination of the superstrate decreases with the increase in the distance of the parasitic element from the source. Further, with the increase in the distance of parasitic element, the enhancement in the gain/directivity tends to be saturated. On this basis, it is stated that the most of the radiated power is due to elements placed in the vicinity of the primary source

and each superstrate element near the source is equally illuminated. In this case, the half-power beam-width and the directivity of the antenna as shown in Fig. 1 are related to the number of unit-cells by the expression [30].

$$\phi_{xz} = \frac{2.65\lambda}{M\pi \wedge_x} \tag{3}$$

$$\phi_{yz} = \frac{2.65\lambda}{N\pi \wedge_y} \tag{4}$$

In the Eqs. (3) and (4), ϕ_{xz}, ϕ_{yz}, M, N, $\wedge_x$, $\wedge_y$ are the half-power beam-width in xz-plane, half-power beam-width in yz-plane, number of unit cells along x-axis, number of unit cells along y-axis, periodicity along x-axis and periodicity along y-axis, respectively. The broadside directivity ($\theta = 0°$) of the antenna in the far-field is approximated by following mathematical expressions.

$$D \approx \frac{4\pi}{2\phi_{xz}\phi_{yz}} \tag{5}$$

or

$$D \approx \frac{8.83MN \wedge_x \wedge_y}{\lambda^2} \tag{6}$$

or

$$D \approx \frac{8.83A}{\lambda^2} \tag{7}$$

and

$$D_{dB} \approx 10 \log \frac{8.83A}{\lambda^2} (\text{in dB}) \tag{8}$$

In the Eqs. (5)–(8), D, A, and D_{dB} are the directivity of the antenna, total surface area of the superstrate and directivity in dBi, respectively.

3 Prediction of directivity at terahertz frequency

To validate the theory presented in the Sect. 2, we have investigated a probe-fed rectangular microstrip antenna with two different sets of unit-cell array size at 600 GHz in this section.

3.1 Analysis of the frequency selective surface

A capacitive FSS unit-cell is shown in Fig. 2. The reflective surface of the unit-cell is made of copper ($\sigma = 5.8 \times 10^7$ S/m) whose length, width and thickness (t) are 152, 110 and 20 μm, respectively. The reflective surface is supported by a 50 μm thick low-dielectric permittivity PTFE ($\varepsilon_r = 2.08$ and $\tan\delta = 0.0004$) material. The length and width of the supporting dielectric are 160 and 120 μm along x- and y-axis, respectively.

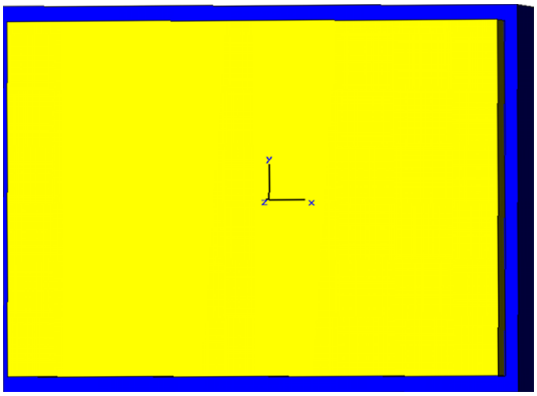

Fig. 2 The unit-cell of the FSS with support

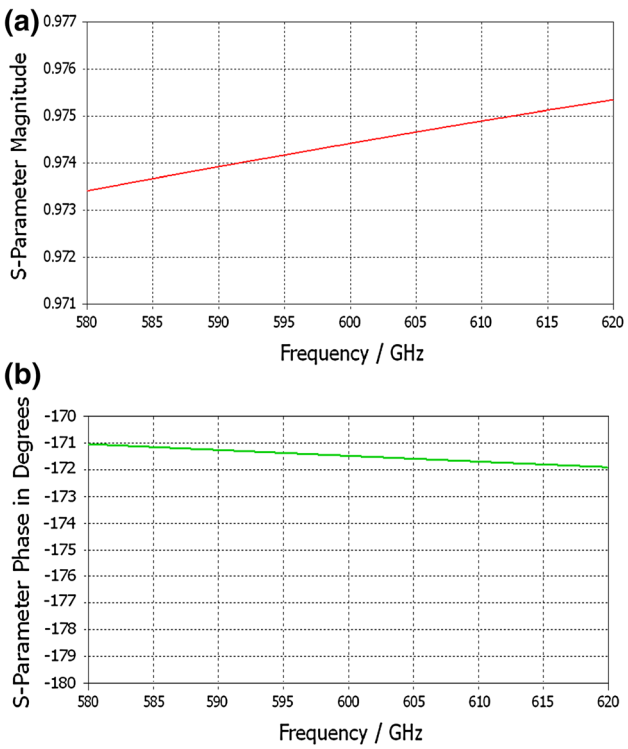

Fig. 3 The reflection coefficient **a** magnitude and **b** phase angle of the unit-cell

The reflection phase and magnitude of the FSS unit-cell is shown in Fig. 3 which reveals that the magnitude of the reflection coefficient ($|\Gamma|$) > 0.97 and phase angle at 600 GHz is $-171.5°$. The value of 'h' as shown in Fig. 1 is computed by using Eqs. (1) and (2) and it is 200 μm to achieve the resonance of the antenna at this frequency.

3.2 Geometrical configuration of antenna

A simple rectangular patch antenna along with the FSS array is shown in Fig. 1. The length of the patch along x-axis, width of the patch along y-axis and thickness of the patch along z-axis are equal to 152, 110 and 20 μm, respectively. The patch

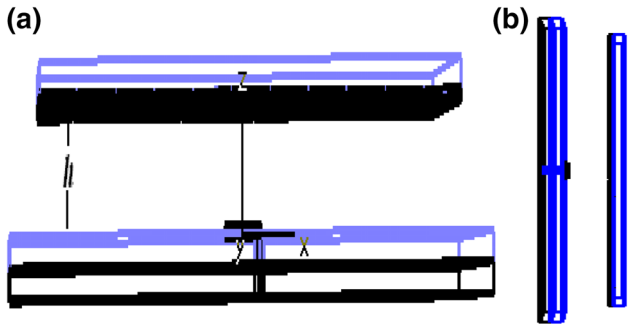

Fig. 4 Schematic of the antenna with 11 × 15 unit cells **a** *bottom* and **b** *side view*

is placed on a 50 μm PTFE substrate material. The substrate is followed by a 20 μm thick copper ground plane and the superstrate (FSS) along with its support is placed at the height '*h*' above the substrate material. The antenna system is fed by a 5 μm radius cylindrical copper probe which is placed 70 μm away from the centre of the patch along x-axis.

3.3 The effect of the number of cells on the directivity

To show the relationship between the number of unit-cells/ superstrate area to the directivity of FSS antenna, we have analyzed two antenna systems.

3.3.1 Superstrate with 11 × 15 *unit-cells*

The structure in this case is shown in Fig. 4. The number of unit-cells along x- and y-axis are $M = 11$ and $N = 15$, respectively. The periodicity of array along x- and y-axis are 160 and 120 μm, respectively. The size of substrate and ground plane is 2000 × 2000 μm^2 ($16\lambda^2$). The substrate and ground plane size have been selected in such a way that they completely cover the superstrate.

The beam-width of the antenna in XZ- and YZ-plane is obtained by using Eqs. (3) and (4), which is equal to 13.45° and 12.3°, respectively. Further, the directivity of antenna calculated by Eqs. (6) and (8) is 20.49 dBi. To validate the analysis, the structure has been simulated by using CST Microwave Studio and the radiation pattern obtained by this simulation is shown in Fig. 5. The simulated half-power beam-width of the major lobe of the antenna in XZ- and YZ- planes are 13.9° and 13.7°, respectively.

Figure 5 shows that the simulated directivity of antenna at 600 GHz is 18.5 dBi. The deviation between predicted and simulated value of the directivity and beam-width arises due to the leakage of energy as the formed cavity is small to encompass all the radiated energy. Moreover, the side-lobes are significant in $\pm 40° \leq \theta \leq \pm 60°$ ranges which can be reduced by increasing the superstrate, substrate and ground plane size. However, the main objective is to relate

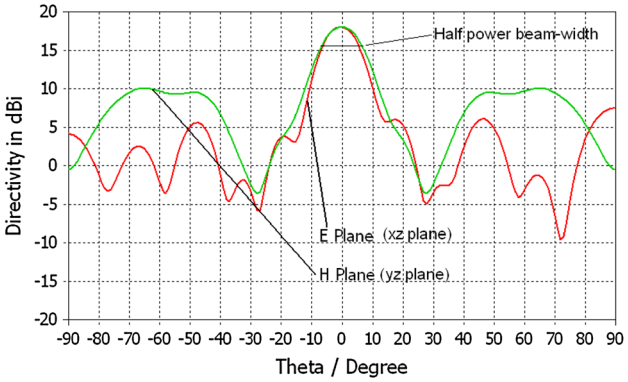

Fig. 5 The radiation pattern of 11 × 15 FSS array superstrate antenna at 600 GHz

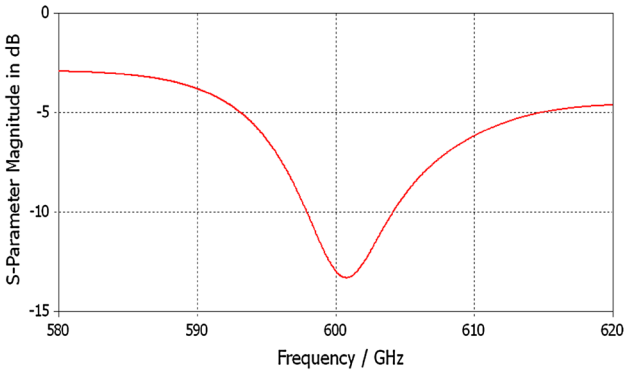

Fig. 6 S_{11} parameter of the proposed antenna as shown in Fig. 4

the number of unit-cells to the directivity of antenna and it is obtained. The S_{11}parameter of the antenna is shown in Fig. 6. The resonance is achieved at $h = 205$ μm instead of 200 μm. However, they are again comparable. The −10 dB impedance bandwidth of the antenna is 6.12 GHz.

3.3.2 Superstrate with 16 × 29 *unit-cells*

In this example, the size of FSS array has been increased to 16 × 29 cells and to cover the superstrate area, the size of the ground plane and substrate has also been increased to 4000 × 4000 μm^2 ($64\lambda^2$).However, other geometrical parameters of the antenna are remain unchanged. The top-view of antenna is shown in Fig. 7.

In this case, the computed half-power beam-width of the antenna in XZ and YZ planes is 7.8° and 8.6°, respectively. The computed directivity of the antenna is 24.97 dBi. The simulated radiation pattern obtained by using CST Microwave Studio is shown in Fig. 8 which reveals that the beam-shape is improved in $\pm 40° \leq \theta \leq \pm 60°$. The directivity of antenna obtained by simulating the structure with CST Microwave Studio is 24.37 dBi which is comparable to that of the predicted value. However, in this case the peak directivity is achieved at 592 GHz instead of 600 GHz and

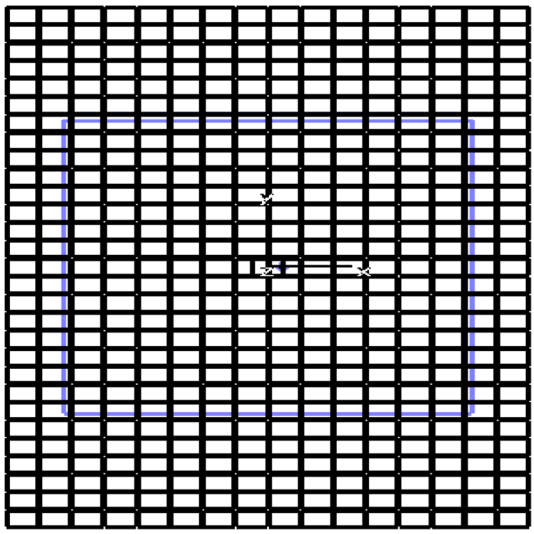

Fig. 7 The *top-view* of the 16 × 29 unit-cell antenna

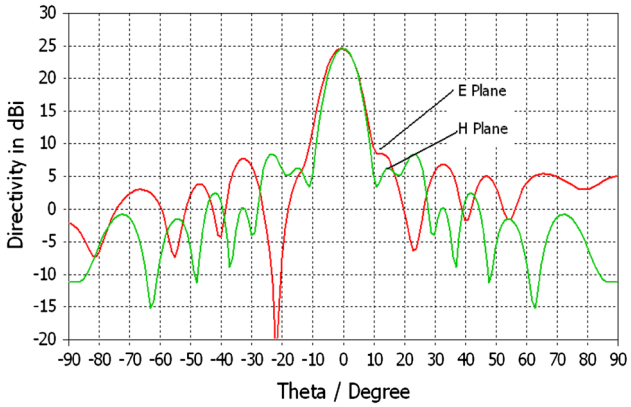

Fig. 8 The directivity of the antenna with 16 × 29 unit-cells

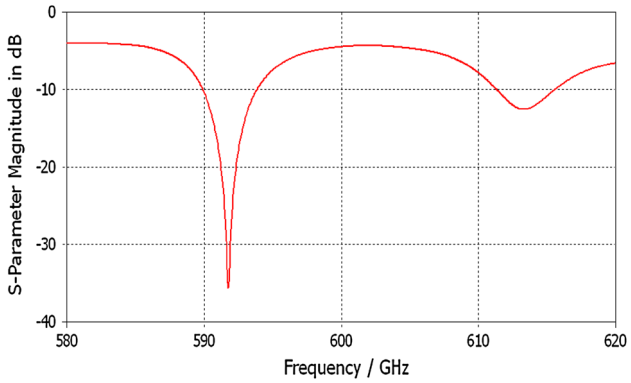

Fig. 9 S_{11} parameter of the 16 × 29 unit-cell FSS array antenna

the $S_{11}$of the antenna is shown in Fig. 9. This downshift in the resonance frequency is due to the superstrate loading and the change in the effective dielectric permittivity of the media within the cavity [26]. However, the analytical and simulated directivity are comparable at the resonance frequency.

To validate the uniform planar array model of the proposed FSS array antenna presented in this paper, we have also computed the directivity of the antenna at resonance by using the ray-tracing method. According to this model, the directivity of the cavity is given as [2,31]:

$$D = \frac{1 + |\Gamma_{FSS}(f, \theta = 0°)|}{1 - |\Gamma_{FSS}(f, \theta = 0°)|} \tag{9}$$

In this case, the broadside directivity of the cavity is predicted by the analysis of reflection coefficient magnitude ($|\Gamma_{FSS}|$) of the unit-cell and the total directivity (in dBi) is obtained by adding the directivity of the primary source to this. On this way, the magnitude of reflection co-efficient of the unit-cell is obtained from Fig. 3a and it is 0.97 and the computed directivity of the cavity is 18 dBi. When a microstrip antenna whose directivity lies in between 6 and 7 dBi is used as a primary source the total expected directivity is 24–25 dBi and it is again comparable with the predicted directivity of the antenna.

4 Validation of numerical model at microwave frequency

To validate the proposed theory in the preceding Sections, we have applied this numerical technique on two recently reported works [26,30].

4.1 Design example-1

Foroozesh and Shafai [29] have investigated various parameters of the probe-fed cavity type microstrip patch antenna and have found the effect of FSS superstrate area on the directivity of antenna. When we apply the proposed method to the already investigated structure, the response is similar. In Figs. 8a and 9 of the reported literature [29], the authors have demonstrated the directivity of the antenna for different superstrate area. We have used Eqs. (7) and (8), and obtained the similar result which is presented in Table 1. Table 1 depicts that the analyzed directivity of the proposed antenna is comparable with that of [29].

Table 1 Comparison of results of reported literature

From Ref. [29]				Directivity (dBi) by proposed method
S. No.	Size of FSS array cm^2	Resonance frequency	Directivity (dBi)	
1.	5 × 5	8.88	12.8	12.8
2.	15 × 15	8.30	21.0	21.85
3.	21 × 21	8.30	24.77 (Appx.)	24.77

4.2 Design example-2

In this example, we have referred the work of Feresidis et. al. [32], in which the authors have investigated partially reflective surface (PRS) and artificial magnetic conductor (AMC) type surfaces. However, we are concerned only about PRS type antenna and its detail explanation can be found in the said literature ([32] Fig. 3a, Sect. 4.1, Fig. 9b, Sect. 4.2). The analysis of the antenna has been carried out at 14 GHz. In this case, the size of reflective surface and the support to the unit-cell are equal to 10×10 and 11×11 mm^2 for the PRS structure, respectively. To enhance the directivity of antenna, total 9×9 patches have been used in the design of the PRS as superstrate. On this way, the computed directivity of the antenna by using Eqs. (6) and (8) at the resonance frequency is 22.76 dBi against 20.5 dBi reported in the literature [32]. The deviation is attributed to the various losses and especially to the size of the cavity.

5 Conclusion

In this paper, we have established a relationship between the number of unit-cells used in a FSS array superstrate antenna and its directivity at the resonance frequency. From this analysis, it is revealed that the directivity of antenna at the resonance frequency can be predicted by the knowledge of the unit-cell geometry and its periodicity. On this way, a generic solution to this problem is presented in this paper. Interestingly, in the analysis of the antenna, various commercial simulation software like CST Microwave Studio in the present work, Ansoft HFSS in [29], and Microstripes in [32] have been used and all these results are comparable with the proposed method. However, the analysis indicates that the directivity of cavity type antenna with capacitive patch FSS can be predicted by using the uniform planar array concept.

Acknowledgments The authors are sincerely thankful to anonymous reviewers for the critical comments and suggestions to improve the quality of the manuscript.

References

1. Balanis, C.A.: Antenna theory analysis and design. Wiley, New York (2001)
2. Von Trentini, G.: Partially reflecting sheet arrays. IRE Trans. Antennas Propag. **4**, 666–671 (Oct. 1956)
3. Zhao, T., Jackson, D.R., Williams, J.T., Oliner, A.A.: General formulas for 2-D leaky-wave antennas. IEEE Trans. Antennas Propag. **53**, 3525–3533 (2005)
4. Liu, Z.G.: Fabry–Perot resonator antenna. J. Infrared Millim. Terahertz Waves **31**(4), 391–403 (2010)
5. Liu, Z.G., Ge, Z.C., Chen, X.Y.: Research progress on Fabry–Perot resonator antenna. Int. J. Zhejiang Univ. Sci. A **10**(4), 583–588 (2009)
6. Boutayeb, H., Tarot, A.C.: Internally excited Fabry–Perot type cavity: power normalization and directivity evaluation. IEEE Antenna Wirel. Propag. Lett. **5**(1), 159–162 (2006)
7. Guerin, N., Enoch, S., Tayeb, G., Sabouroux, P., Vincent, P., Legay, H.: A metallic Fabry–Perot directivity antenna. IEEE Trans. Antennas Propag. **54**(1), 220–224 (2006)
8. Boutayeb, H., Denidni, T.A., Mahdjoubi, K., Tarot, A.C., Sebak, A.R., Talbi, L.: Analysis and design of a cylindrical EBG based directive antenna. IEEE Trans. Antennas Propag. **54**(1), 211–219 (2006)
9. Gadelli, R., Albani, M., Capolino, F.: Array thining by using antennas in a Fabry–Perot cavity for gain enhancement. IEEE Trans. Antennas Propag. **54**(7), 1979–1990 (2006)
10. Ge, Z.C., Zhang, W.X., Liu, Z.G., Gu, Y.Y.: Broadband and high-gain printed antennas constructed from Fabry–Perot resonator structure using EBG or FSS cover. Microw. Opt. Tech. Lett. **48**(7), 1272–1274 (2006)
11. Weily, R., Bird, T.S., Guo, Y.J.: A reconfigurable high-gain partially reflecting surface antenna. IEEE Trans. Antennas Propag. **56**(11), 3382–3390 (2008)
12. Foroozesh, A., Shafai, L.: Effects of artificial magnetic conductors in the design of low-profile high-gain planar antennas with high-permittivity dielectric superstrate. IEEE Antennas Wireless Propag. Lett. **8**, 10–13 (2009)
13. Ju, J., Kim, D., Choi, J.: Fabry–Perot cavity antenna with lateral metallic walls for WiBro base station applications. Electron. Lett. **45**(3), 141–142 (2009)
14. Jha, K.R., Singh, G.: Terahertz dipole antenna in Fabry–Perot cavity with two side-walls to enhance the directivity. Procedings of 35th Infrared Millimetre and Terahertz Waves, Rome, Italy, Sep. 05–08, 2010, pp. 1–2.
15. Kim, G.-J., Han, W.-K., Kim,J.-II, Jeon, S.-G.: High resolution terahertz imaging (T-ray) with a horn antenna. Procedings of 35th Infrared Millimetre and Terahertz Waves, Rome, Italy, Sep. 05–08, 2010, pp. 1–2.
16. Laskar, J., Pinel, S., Dawn, D., Sarkar, S., Perumana, B., Sen, P.: The next wireless waves is a millimeter wave. Micow. J **50**(8), 22–36 (2007)
17. Siegel, P.H.: THz technology. IEEE Trans. Microw. Theory Tech. **50**(3), 910–928 (2002)
18. Pieiewicz, R., Jacob, M., Koach, M., Schoebel, J., Kuner, T.: Performance analysis of future multigigabit wireless communication systems and THz frequency with highly directive antennas in indoor environments. IEEE J. Sel. Top. Quantum Electron. **14**(2), 421–430 (2008)
19. Formanek, F., Burn, M.-A., Umetsu, T., Omari, S., Yasuda, A.: A spheric silicon lenses for terahertz photoconductive antennas. Appl. Phys. Lett. **94**(2), 021113–021113-03 (2009)
20. Filipovic, D.F., Gearhart, S.S., Rebeiz, G.N.: Double-slot antennas on extended hemispherical and elliptical silicon lens dielectric lenses. IEEE Trans. Microw. Theory Tech. **41**(10), 1738–1749 (2003)
21. Han, K., Nguyen, T.K., Park, I., Han, H.: Terahertz Yagi-Uda antenna for high input resistance. J. Infrared Millim. Terahertz Waves **31**(4), 441–454 (2010)
22. Jha, K.R., Singh, G.: Dual-band rectangular microstrip patch antenna at terahertz frequency for surveillance system. J. Comput. Electron. **9**(1), 31–41 (2010)
23. Jha, K.R., Singh, G.: Analysis and design of enhanced directivity microstrip antenna at terahertz frequency by using electromagnetic bandgap material. Int. J. Numer. Model. **24**(5), 410–424 (2011)
24. Jha, K.R., Singh, G.: Design of highly directive cavity type terahertz antenna for wireless communication. Opt. Commun. **284**(20), 4996–5002 (2011)

25. Jha, K.R., Singh, G.: Ring resonator integrated hemi-elliptical lens antenna at terahertz frequency. Opt. Commun. **285**(16), 3445–3452 (2012)
26. Jha, K.R., Singh, G.: Microstrip patch array antenna on photonic crystal substrate at terahertz frequency. Infrared Phys. Technol. **55**(1), 32–39 (2012)
27. Piesiewicz, R., Islam, M.N., Koch, M., Kurner T.: Towards short-range terahertz communication systems: basic considerations. Procedings of 18th International conference on Applied electromagnetics and communications, Dubrovnik, Croatia, Oct. 12–14, 2005.
28. Foroozesh, A., Shafai, L.: 2-D truncated periodic leaky-wave antennas with reactive impedance surface ground. Procedings of IEEE AP-S Int. Symp., Albuquerque, NM, Jul. 9–14, 2006, pp. 15–18.
29. Foroozesh, A., Shafai, L.: Investigation into the effects of patch-type FSS superstrate on the high-gain cavity resonance antenna design. IEEE Trans. Antennas Propag. **58**(2), 258–270 (2010)
30. Collin, R.E.: Antennas and radiowave propagation. McGraw Hill International, New York (1985)
31. Feresidis, A.P., Vardaxoglou, J.C.: High gain planar antenna using optimised partially reflective ssurfaces. Proc. Inst. Electron. Eng. Microw. Antennas Propag. **48**(6), 345–350 (2001)
32. Feresidis, A.P., Goussetis, G., Wang, S., Vardaxoglou, J.C.: Artificial magnetic conductor surfaces and their application to low-profile high gain planar antenna. IEEE Trans. Antennas propag. **53**(1), 209–215 (2005)